

Thermodynamic-consistent multiple-relaxation-time lattice Boltzmann equation model for two-phase hydrocarbon fluids with Peng-Robinson equation of state

Zhonghua Qiao^a, Xuguang Yang^{a,b,*}, Yuze Zhang^a

^a*Department of Applied Mathematics, The Hong Kong Polytechnic University, Hung Hom, Hong Kong*

^b*School of Mathematics and Computational Science, Hunan First Normal University, Changsha, P. R. China*

Abstract

In this work, a multiple-relaxation-time (MRT) lattice Boltzmann (LB) equation model with Beam-Warming (B-W) scheme is proposed to simulate a multi-phase fluid system with Peng-Robinson (P-R) equation of state (EOS). The mathematical model of the multi-phase fluid flow is derived based on the NVT-based framework, where the Helmholtz free energy of P-R EOS is introduced. The nonideal force in the multi-phase flow is directly computed from the free energy in order to obtain a more compact formulation of hydrodynamic equations, which is termed as potential form. The MRT-LB model is developed based on the potential form of hydrodynamic equations, which can eliminate spurious currents effectively. In addition, to capture the tiny nonconvex perturbation from the linear trend of P-R model precisely, the B-W scheme is utilized in the present MRT-LB model, which gives rise to an adjustable Courant-Friedrichs-Lewy (CFL) number. Also, the second order accuracy can be naturally achieved by this scheme without any other requirements and numerical boundary conditions. In the numerical experiments, a realistic hydrocarbon component (isobutane) in three dimensional space is simulated by the proposed MRT-LB model. Numerical results show that the magnitude of spurious currents can be significantly reduced by the present MRT-LB model. In addition, our numerical predictions of surface tension agree well with the experimental data, which verify the effectiveness of the proposed MRT-LB model.

Keywords: multi-phase fluid flow, diffuse interface model, Peng-Robinson equation of state, MRT lattice Boltzmann method

1. Introduction

In the petroleum industry, multi-phase fluid flow in porous media is of great interest since it widely exists in various producing processes, such as gas injection and secondary oil recovery, especially shale gas reservoir, which has become an increasingly important source of natural gas in recent years. A deep understanding of phase behavior of reservoir fluid flow in porous media is a basic foundation to predict oil and gas production.

*Corresponding author

Email addresses: zhonghua.qiao@polyu.edu.hk (Zhonghua Qiao), xuguangcscs@hust.edu.cn (Xuguang Yang), 16903152r@connect.polyu.hk (Yuze Zhang)

Among many numerical simulations of porous media flows, pore scale simulations can provide detailed local information on fluid distribution and velocity, which is important for understanding the fundamental mechanism of porous media flows. The LB method, which has emerged as an alternative to classical computational fluid dynamics (CFD) techniques, has been successfully applied to pore scale simulations of multiphase flow in porous media [1–4]. The LB method is derived from the kinetic Boltzmann equation, which can be regarded as a numerical method based on mesoscopic theory that connects the microscopic and macroscopic descriptions of the dynamics. The kinetic nature of LB method makes the inter-molecular interactions to be easily incorporated into a LB equation model, so that it becomes a suitable candidate to simulate a multi-phase system. A variety of complex physical problems have been studied by the multiphase LB method, such as the works in references [5–7]. Up to now, several types of LB models for multi-phase flows have been successfully developed from different theoretical backgrounds, such as color gradients LB model [8], the pseudopotential LB model [9, 10], free energy model [11–13], the kinetic model based on Enskog equation [14, 15] and the phase field based LB model [16–20]. On the macroscopic level, most of these multiphase LB models can be classified as diffuse interface models. The basic idea of the diffuse interface model is to treat the phase interface as a transitional region with nonzero thickness, where fluid properties vary smoothly across the interface [21, 22]. Thus, the interface curvature and the complex interfacial dynamics can be resolved with higher accuracy. These features make the diffuse interface model ideally suitable for predicting the phase behavior of reservoir fluids.

In the diffuse interface based LB model, a double well potential form of the free energy density is widely used to simulate binary fluid systems [23–25]. However, it is hardly to set meaningful quantitative parameters of the double well potential form to simulate realistic hydrocarbon species in oil-gas fluid systems. In order to capture interfacial properties of these systems accurately, the free energy model of Peng-Robinson (P-R) equation of state (EOS) has been introduced. Recently, the diffuse interface model with P-R EOS has been widely studied and applied to describe real states of hydrocarbon fluids in the petroleum industry [26, 27]. Several energy stable numerical methods, such as convex-splitting scheme and the recently developed Invariant Energy Quadratization (IEQ) approach, have been implemented to study the diffuse interface model with P-R EOS [28–31]. In these works, the single-component two phase fluid systems were numerically studied in 2D and 3D spaces. While for a multi-component hydrocarbon system, Fan et al. [32] developed a component-wise convex splitting scheme to solve it. In their work, both Van der Waals and P-R equation of states (EOSs) were investigated. Besides aforementioned works, which focus on the equilibrium state of the interfacial behavior, there have been several efforts devoted to the general mathematical model of multi-component two-phase fluid flow with P-R EOS. Such as the work of Kou and Sun [33], the multi-component two-phase flow problems with partial miscibility based on a realistic EOS were numerically studied by a multi-scale simulation method. Furthermore, using the moles, volume and temperature (so-called NVT-based framework) as the primal state variables, Kou et al. [34] developed a general diffuse interface model with a realistic EOS to describe the multi-component two phase fluid flow and an energy-dissipation numerical scheme was also designed to solve

it. It can be seen from works mentioned above that a variety of numerical schemes have been successfully applied to solve the diffuse interface model with P-R EOS. However, due to the strong nonlinearity and high stiffness of the energy functional of P-R fluids, most of these existing numerical methods were developed for the static behaviors of two phase fluid systems or two dimensional fluid flow. Considering the complex transport process of hydrocarbon fluids in subsurface, the efficient and easy-to-implement numerical schemes still needs to be developed for more general and three dimensional multiphase fluid systems with realistic EOS.

In this work, the lattice Boltzmann (LB) method is applied to simulate nonideal fluids with P-R EOS. In the diffuse interface based LB model, how to incorporate realistic EOS, which is consistent with thermodynamic theory, is crucial for the simulation of nonideal fluid systems. Besides, it is also very important to eliminate the spurious current in the vicinity of a curve interface in the implementation of multi-phase LB model. In the literature, Wagner [35] demonstrated that using potential form other than pressure form for the surface force could remove the spurious current near a circular bubble to machine accuracy. In most existing multi-phase LB models, the potential form of the surface force is derived from the popular double-well potential free energy or the free energy based on van der Waals EOS. While in the simulation of realistic hydrocarbon species in multi-phase fluid systems, the free energy of P-R EOS should be used. In the present work, based on the NVT framework, the Helmholtz free energy of P-R EOS is adopted in the diffuse interface model. Through using primal thermodynamical relations, general hydrodynamic equations for describing nonideal fluids with P-R EOS are derived. Furthermore, based on the relation between the pressure gradient and chemical potential gradient, the potential form of momentum balance equation is developed, where the gradient of chemical potential becomes the primary driving force of the fluid motion. The derived model brings great challenges to the construction of numerical schemes. The main difficulties are the strong nonlinearity of Helmholtz free energy density and tight coupling relations between molar densities and velocity. To solve these problems, a multiple-relaxation-time (MRT) lattice Boltzmann equation model with Beam-Warming (B-W) scheme is proposed in this work. The MRT model or generalized LB model was proposed by d’Humières in 1992 [36]. After that, Lallemand and Luo [37] have extended this model in the moment space rather than in the discrete velocity space. Different from the single-relaxation-time collision model (also called the Bhatnagar-Gross-Krook (BGK) model), which uses a relaxation process with a single relaxation time to characterize collision effects, a collision matrix with different relaxation times is adopted in the MRT model during the collision process. Because of various relaxation processes, the MRT model is more flexible to incorporate additional physics that cannot be naturally represented by the LBGK model. It is well known that multi-phase flows involve additional physical complexity as a result of interfacial physics involved, i.e., phase segregation and surface tension effects. Naturally, to handle this complex multi-phase fluid system with P-R EOS, the MRT collision operator is utilized in the proposed LB equation model. In addition, as mentioned in [31], the free energy of P-R EOS is a tiny nonconvex perturbation from a linear trend that causes phase separation. Therefore, it needs to be captured accurately. In this work, to resolve the molar

densities more accurate, the B-W propagation scheme is developed base on the MRT model, which gives rise to an adjustable Courant-Friedrichs-Lewy (CFL) number. The second order accuracy can be naturally achieved by this scheme without any other requirements and numerical boundary conditions.

The rest of this paper is organized as follows. In Section 2, general hydrodynamic equations for non-ideal fluids with P-R EOS is derived based on thermodynamical relations. Whereafter, the MRT-LB equation model with B-W scheme for the general equations is proposed in Section 3. In Section 4, a series of numerical experiments are carried out to verify the effectiveness of the proposed MRT-LB model and the numerical scheme. Finally, some conclusions are given in Section 5.

2. Mathematical model of nonideal fluids with Peng-Robinson equation of state

In this section, the P-R free energy model is introduced. Based on the fundamental functions of thermodynamics, a general model for the nonideal fluids flow with P-R EOS is given, in which the viscosity and density gradient contribution to free energy are under consideration.

2.1. Helmholtz free energy for a realistic equation of state

For realistic fluids, diffuse interfaces always exist between two phases. To describe this feature, a local density gradient contribution is introduced into the Helmholtz free energy of inhomogeneous fluids. The total Helmholtz free energy is the summation of two contributions: Helmholtz free energy of bulk homogeneous fluid and a local density gradient contribution:

$$\begin{aligned} F(\mathbf{n}; T, \Omega) &= F_0(\mathbf{n}; T, \Omega) + F_{\nabla}(\mathbf{n}; T, \Omega) \\ &= \int_{\Omega} f_0(\mathbf{n}; T) d\mathbf{x} + \int_{\Omega} f_{\nabla}(\mathbf{n}; T) d\mathbf{x}. \end{aligned} \quad (1)$$

$f_0(\mathbf{n})$ is the Helmholtz free density of bulk homogeneous fluid, $f_{\nabla}(\mathbf{n})$ is the contribution of Helmholtz free energy density from the concentration gradient and $\mathbf{n} = (n_1, n_2, \dots, n_M)$. For a single component two phase fluid system, $f_{\nabla}(\mathbf{n})$ can be expressed by a simple quadratic relation:

$$f_{\nabla}(n) = \frac{1}{2} \kappa \nabla n \cdot \nabla n, \quad (2)$$

where κ is the pure component influence parameter.

The homogeneous term $f_0(n)$ can be computed by using the equation of state. In this study, P-R EOS, which is widely used in the oil reservoir and chemical engineering, is considered. $f_0(n)$ is expressed as summation of two terms, ideal part and excess one [31],

$$f_0(n) = f_0^{ideal}(n) + f_0^{excess}(n), \quad (3a)$$

$$f_0^{ideal}(n) = RTn(\ln n - 1), \quad (3b)$$

$$f_0^{excess}(\mathbf{n}) = -nRT \ln(1 - bn) + \frac{an}{2\sqrt{2}b} \ln\left(\frac{1 + (1 - \sqrt{2})bn}{1 + (1 + \sqrt{2})bn}\right). \quad (3c)$$

In the above expressions, R denotes the universal gas constant which is approximate $8.31432JK^{-1}mol^{-1}$. The parameter a is related to inter-particle attractive force between a couple of particles and b is associated with the size of each particle. κ is defined by these two parameters [38]. The specific definition of these parameters are given in Appendix A.

The pressure of homogeneous fluids p_0 is related to the Helmholtz free energy $f_0(n)$ in the following way

$$p_0 = n\left(\frac{\partial f_0}{\partial n}\right) - f_0 = n\mu_0 - f_0. \quad (4)$$

The homogeneous chemical potential μ_0 can be expressed as the following nonlinear form

$$\mu_0 = RT \ln \frac{n}{1 - bn} + RT \frac{bn}{1 - bn} + \frac{a}{2\sqrt{2}b} \ln\left(\frac{1 + (1 - \sqrt{2})bn}{1 + (1 + \sqrt{2})bn}\right) - \frac{an}{1 + bn + bn(1 - bn)}. \quad (5)$$

Replacing f_0 and μ_0 by (3) and (5), we have the P-R EOS [39],

$$p_0 = \frac{nRT}{1 - bn} - \frac{n^2 a(T)}{1 + 2bn - b^2 n^2}. \quad (6)$$

The total chemical potential μ is defined as

$$\mu = \frac{\delta f(n)}{\delta n} = \mu_0 - \kappa \nabla^2 n. \quad (7)$$

Furthermore, the general pressure can be formulated as

$$p = n\mu - f = n(\mu_0 - \kappa \nabla^2 n) - (f_0 + \frac{1}{2} \kappa \nabla n \cdot \nabla n) = p_0 - \kappa n \nabla^2 n - \frac{1}{2} \kappa \nabla n \cdot \nabla n. \quad (8)$$

2.2. Hydrodynamic equations of nonideal fluids

The hydrodynamic equations for the nonideal fluids are

$$\frac{\partial \rho}{\partial t} + \nabla \cdot (\rho \mathbf{u}) = 0. \quad (9)$$

The momentum balance equation is

$$\rho \left(\frac{\partial \mathbf{u}}{\partial t} + \mathbf{u} \cdot \nabla \mathbf{u} \right) = -\nabla p + \nabla \cdot (\eta (\nabla \mathbf{u} + \nabla \mathbf{u}^T)) + (\xi - \frac{2}{D} \eta) (\nabla \cdot \mathbf{u}) \mathbf{I} - \nabla \cdot (\kappa \nabla n \otimes \nabla n). \quad (10)$$

Using the following formula

$$n \nabla \mu = \nabla p + \kappa \nabla \cdot (\nabla n \otimes \nabla n),$$

the above equation can be reformulated as a more compact form, which is termed as the *potential form*,

$$\frac{\partial \rho \mathbf{u}}{\partial t} + \nabla \cdot (\rho \mathbf{u} \otimes \mathbf{u}) = -n \nabla \mu + \nabla \cdot (\eta (\nabla \mathbf{u} + \nabla \mathbf{u}^T)) + (\xi - \frac{2}{D} \eta) (\nabla \cdot \mathbf{u}) \mathbf{I}, \quad (11)$$

where $\mu = \mu_0 - \kappa \nabla^2 n$. According to the relation $\nabla p_0 = n \nabla \mu_0$, the momentum balance equation can also be referred to as the *pressure form*

$$\frac{\partial \rho \mathbf{u}}{\partial t} + \nabla \cdot (\rho \mathbf{u} \otimes \mathbf{u}) = -\nabla p_0 + \nabla \cdot (\eta (\nabla \mathbf{u} + \nabla \mathbf{u}^T)) + (\xi - \frac{2}{D} \eta) (\nabla \cdot \mathbf{u}) \mathbf{I} + \kappa n \nabla^2 n. \quad (12)$$

Although the two formulations are totally identical mathematically, their discrete versions may differ slightly due to some discretization errors, and may have significant influences on the spurious currents [35, 40]. It is worth noting that the above hydrodynamic equations are the general model for the diffuse interface two phase fluid system. Any other realistic EOS can be incorporated into this model, once the corresponding Helmholtz free energy density is known.

3. Lattice Boltzmann equation model for hydrodynamic equations

In the present work, the LBM with MRT collision operator is applied to solve the hydrodynamic equations (9) and (11). In particular, to capture the tiny nonconvex perturbation from the linear trend of Peng-Robinson model precisely, the Beam-Warming scheme is used in the present MRT-LBM.

The discrete velocity Boltzmann equation with MRT collision operator can be expressed as

$$\frac{\partial g_i}{\partial t} + \mathbf{c}\mathbf{e}_i \cdot \nabla g_i = -\Lambda_{ij}[g_j - g_j^{eq}] + G_i, \quad (13)$$

where, $g_i(\mathbf{x}, t)$ is the discrete distribution function of particle at site \mathbf{x} and time t moving with speed c along the direction \mathbf{e}_i and $\mathbf{c}\mathbf{e}_i = c\mathbf{e}_i$, $\{\mathbf{e}_i, i = 0, \dots, k - 1\}$ is the set of discrete velocity directions, c is the sound speed, Λ_{ij} is the collision matrix, $g_i^{eq}(\mathbf{x}, t)$ is the equilibrium distribution function (EDF), and G_i is the force distribution function. We now solve this discrete velocity Boltzmann equation using a time-splitting scheme. Then, Eq. (13) is decomposed into two subprocesses, i.e., the collision process,

$$\frac{\partial g_i}{\partial t} = -\Lambda_{ij}[g_j - g_j^{eq}] + G_i, \quad (14)$$

and the streaming process,

$$\frac{\partial g_i}{\partial t} + \mathbf{c}\mathbf{e}_i \cdot \nabla g_i = 0. \quad (15)$$

In the MRT model, the collision subprocess can be carried out in the moment space. Without loss of generality, we take the generally used *D2Q9* model as an example. The distribution functions g_i in moment space are defined as

$$\mathbf{m} = \mathbf{M} \cdot \mathbf{g} = (\rho, e, \varepsilon, j_x, q_x, j_y, q_y, p_{xx}, p_{xy})^T,$$

where e and ε are related to total energy and the function of energy square; j_x and j_y are relevant to the momentum; q_x and q_y are related to the x and y components of the energy; p_{xx} and p_{xy} are the corresponding diagonal and off-diagonal components of the stress tensor, respectively. \mathbf{M} is the transformation matrix, for

the $D2Q9$ model, \mathbf{M} is defined as

$$\mathbf{M} = \begin{pmatrix} 1 & 1 & 1 & 1 & 1 & 1 & 1 & 1 & 1 \\ -4 & -1 & -1 & -1 & -1 & 2 & 2 & 2 & 2 \\ 4 & -2 & -2 & -2 & -2 & 1 & 1 & 1 & 1 \\ 0 & 1 & 0 & -1 & 0 & 1 & -1 & -1 & 1 \\ 0 & -2 & 0 & 2 & 0 & 1 & -1 & -1 & 1 \\ 0 & 0 & 1 & 0 & -1 & 1 & 1 & -1 & -1 \\ 0 & 0 & -2 & 0 & 2 & 1 & 1 & -1 & -1 \\ 0 & 1 & -1 & 1 & -1 & 0 & 0 & 0 & 0 \\ 0 & 0 & 0 & 0 & 0 & 1 & -1 & 1 & -1 \end{pmatrix}.$$

With the transformation matrix \mathbf{M} , the collision process can be rewritten onto the moment space as

$$\frac{\partial \mathbf{m}}{\partial t} = -\tilde{\mathbf{S}}(\mathbf{m} - \mathbf{m}^{eq}) + \hat{\mathbf{G}}, \quad (16)$$

where $\tilde{\mathbf{S}} = \mathbf{M}\mathbf{\Lambda}\mathbf{M}^{-1}$ is a diagonal relaxation matrix, given by

$$\tilde{\mathbf{S}} = \text{diag}\{\tilde{s}_0, \tilde{s}_1, \tilde{s}_2, \tilde{s}_3, \tilde{s}_4, \tilde{s}_5, \tilde{s}_6, \tilde{s}_7, \tilde{s}_8\}.$$

Now we define the nondimensional relaxation matrix $\mathbf{S} = \delta t \tilde{\mathbf{S}}$, and then

$$\mathbf{S} = \text{diag}\{s_0, s_1, s_2, s_3, s_4, s_5, s_6, s_7, s_8\}.$$

In simulations, $s_0 = s_3 = s_5$, $s_4 = s_6$ and $s_7 = s_8$. We would like to point out that, if s_i are equal to each other, the MRT model will reduce to the LBGK model.

Discretizing Eq. (16) using the explicit first order Euler scheme leads to

$$\mathbf{m}^+ = \mathbf{m} - \delta t \tilde{\mathbf{S}}(\mathbf{m} - \mathbf{m}^{eq}) + \delta t \hat{\mathbf{G}}, \quad (17)$$

where $\mathbf{m}^+ = \mathbf{M}\mathbf{g}^+$ is the postcollision moments with $\mathbf{g}^+ = (g_0^+, \dots, g_8^+)^T$ being the postcollision distribution function.

The equilibrium moments \mathbf{m}^{eq} are defined as

$$\mathbf{m}^{eq} = \mathbf{M} \cdot \mathbf{g}^{eq} = \rho \begin{bmatrix} 1 \\ -2 + 3\mathbf{u}^2 \\ 1 - 3\mathbf{u}^2 \\ u \\ -u \\ v \\ -v \\ u^2 - v^2 \\ uv \end{bmatrix}. \quad (18)$$

In addition, $\widehat{\mathbf{G}} = \mathbf{M}\mathbf{G}$ are the corresponding force moments, which have the following form

$$\begin{aligned}
\widehat{G}_0 &= 0, \\
\widehat{G}_1 &= 6\left(1 - \frac{s_1}{2}\right)\mathbf{u} \cdot \mathbf{F}_t, \\
\widehat{G}_2 &= -6\left(1 - \frac{s_2}{2}\right)\mathbf{u} \cdot \mathbf{F}_t, \\
\widehat{G}_3 &= F_{tx}, \\
\widehat{G}_4 &= -\left(1 - \frac{s_4}{2}\right)F_{tx}, \\
\widehat{G}_5 &= F_{ty}, \\
\widehat{G}_6 &= -\left(1 - \frac{s_6}{2}\right)F_{ty}, \\
\widehat{G}_7 &= 2\left(1 - \frac{s_7}{2}\right)(uF_{tx} - vF_{ty}), \\
\widehat{G}_8 &= \left(1 - \frac{s_8}{2}\right)(uF_{ty} + vF_{tx}),
\end{aligned} \tag{19}$$

where $\mathbf{G} = (G_0, \dots, G_8)^T$. \mathbf{F}_t is the total external force, which is expressed as

$$\mathbf{F}_t = \mathbf{F}_s + \mathbf{F} = (F_{tx}, F_{ty}).$$

Here \mathbf{F}_s represents the force associated with the surface tension, and \mathbf{F} is the external body force, such as the gravity. For the potential form of the hydrodynamic equations, \mathbf{F}_s should be expressed as

$$\mathbf{F}_s = \nabla(c_s^2\rho) - n\nabla\mu.$$

While for the pressure form, \mathbf{F}_s has the following form

$$\mathbf{F}_s = \nabla(c_s^2\rho - p_0) + \kappa n\nabla\nabla^2 n,$$

110 in which the first term on the right hand side of above equations is to cancel out with the ideal-gas contribution to the pressure.

We solve Eq. (15) on a regular lattice with spacing δx using the second-order Beam-Warming scheme,

$$\begin{aligned}
g_i(\mathbf{x}, t + \delta t) &= g_i^+(\mathbf{x}, t) - \frac{A}{2}(3g_i^+(\mathbf{x}, t) - 4g_i^+(\mathbf{x} - \mathbf{e}_i\delta x, t) + g_i^+(\mathbf{x} - 2\mathbf{e}_i\delta x, t)) \\
&\quad + \frac{A^2}{2}(g_i^+(\mathbf{x}, t) - 2g_i^+(\mathbf{x} - \mathbf{e}_i\delta x, t) + g_i^+(\mathbf{x} - 2\mathbf{e}_i\delta x, t)),
\end{aligned} \tag{20}$$

where $0 < A \leq 1$ is the CFL number [41, 42] and the time step δt is determined from the CFL condition, $\delta t = A\delta x/c$. Different from the LB model with standard propagation scheme (called standard LBM), where the CFL number is fixed to 1, the CFL number is an adjustable parameter in the present scheme.

The macroscopic quantities, ρ and \mathbf{u} are calculated using

$$\rho = \sum_i g_i, \quad \rho\mathbf{u} = \sum_i \mathbf{c}_i g_i + \frac{\delta t}{2}\mathbf{F}_t. \tag{21}$$

Furthermore, in the calculation of the interaction force, some gradients of scalar variables are multiplied by the microscopic velocity set ($\mathbf{e}_i \cdot \nabla$). These terms are treated as directional derivatives along characteristics. The second order central difference (CD) approximation of the directional derivative of a variable ϕ is expressed as

$$\mathbf{e}_i \cdot \nabla^C \phi(\mathbf{x}, t) = \frac{\phi(\mathbf{x} + \mathbf{e}_i\delta x, t) - \phi(\mathbf{x} - \mathbf{e}_i\delta x, t)}{2\delta x}. \tag{22}$$

Derivatives other than the directional derivatives can be obtained by taking moments of the directional derivatives with appropriate weights to ensure isotropy

$$\nabla^C \phi(\mathbf{x}, t) = \frac{1}{c_s^2} \sum_{i \neq 0} \omega_i \mathbf{e}_i \otimes \mathbf{e}_i \cdot \nabla^C \phi(\mathbf{x}, t). \quad (23)$$

The Laplacian term is calculated using the following isotropic differences with second-order accuracy

$$\nabla^2 \phi(\mathbf{x}, t) = \sum_{i \neq 0} \frac{2\omega_i [\phi(\mathbf{x} + \mathbf{e}_i \delta x, t) - \phi(\mathbf{x}, t)]}{(c_s \delta x)^2} \quad (24)$$

115 4. Numerical results

In this section, we will implement a series of numerical simulations to demonstrate the effectiveness of the proposed thermodynamic consistent MRT-LB model and the B-W scheme.

4.1. Accuracy test

In this subsection, numerical experiments are designed in two-dimensional space to test the temporal
 120 accuracy of the proposed MRT-LB model with B-W scheme. The substance isobutane (nC_4) at temperature 350K is simulated. The critical properties, the initial molar densities of liquid n_l and gas n_g , and the normal boiling point of nC_4 are provided in Table C.1. The initial condition is set as: the molar density equals the liquid isobutane under a saturated pressure in the region $[0.3L, 0.7L]$, where $L = 2 \times 10^{-8}$ meters, thus the effect of gravity can be neglected in such scale. The rest of the domain is filled with a saturated isobutane
 125 gas. The periodic boundary condition is imposed.

The 1024×1024 mesh is selected as the benchmark solution for computing errors and the time step is fixed to 1.0×10^{-9} . The following global relative error is used to measure the accuracy:

$$E_\phi = \frac{\sum |\phi(\mathbf{x}, t) - \phi^*(\mathbf{x}, t)|}{\sum |\phi^*(\mathbf{x}, t)|}, \quad (25)$$

where ϕ and ϕ^* are the numerical solution and benchmark one, respectively, and the summation is taken over all grid points. The errors are listed in Table C.2 with different meshes and different CFL numbers. It is shown that the proposed LBM gives second-order accuracy in space and the accuracy is independent on the values of CFL number A.

130 4.2. The two-phase coexistence densities

The two-phase coexistence densities solved by the Maxwell equal-area construction are used as the benchmark to verify the thermodynamic consistency of the numerical multiphase models. With horizontal phase interfaces, the middle part of the domain is initialized as liquid while the remaining part is set as gas. The value of κ is set to be 0.01. The P-R EOS, which is widely used in the oil industries and petroleum engineering, is considered in this work. The parameters are set as $a(T) = \frac{2}{49} [1 + (0.37464 + 1.54226\omega - 0.26992\omega^2) \times$
 135 $(1 - \sqrt{T/T_c})]^2$ with the acentric factor $\omega = 0.344$, $b = 2/21$ and $R = 1$. Thus, the critical temperature and

density are $T_c = 0.072919$ and $\rho_c = 2.657304$, respectively. In simulations, the computational domain is a 127×127 meshgrid with periodical boundary condition, the CFL number A is set to be 0.5, and the D2Q9 lattice model is used. The relaxation parameters can be determined by a linear stability analysis [37]. Noted that s_0, s_3 and s_5 have no influence on the deriving of the hydrodynamic equations. Thus, for simplicity, the relation $s_0 = s_3 = s_5 = 1.0$ is used [43], and $s_7 = s_8 = 1.2$ is corresponded to the kinematic viscosity $\nu = 0.01$. The other relaxation parameters are chosen as: $s_1 = s_2 = 1.0$ and $s_4 = s_6 = 1.7$ [44]. It can be clearly seen from Fig. C.1 that the obtained coexistence densities of P-R EOS are in excellent agreement with the benchmark solutions computed by the Maxwell equal-area construction. These results numerically confirm that the present model is thermodynamically consistent.

4.3. Spurious currents

In this section, a realistic hydrocarbon component of isobutane (nC_4) in three dimensional space is simulated to investigate the spurious currents. The computation domain is $\Omega = (0, L)^3$. The initial condition is to impose the liquid density of hydrocarbons under saturated pressure condition at 350K in the region of $(0.3L, 0.7L)^3$, and the rest of the domain is filled with saturate gas of nC_4 under the same temperature. Following the definition of P-R parameters a, b and the influence parameter κ in Appendix A [45], the values of these parameters can be calculated and list in Table C.1. In the numerical simulation, a $200 \times 200 \times 200$ uniform cubic mesh grid and the D3Q15 lattice model are used. The CFL number $A = 0.08$.

Initially, a cubic bubble is put in the center of the computational domain. As time evolves, the cubic droplet has become a sphere-like shape due to the surface tension (see Fig. C.2). After convergence, the droplet shape appears to be a perfect sphere. Then, we take the average kinetic energy $E = \int \frac{1}{2} \rho |\mathbf{u}|^2 d\mathbf{x}$ as an indicator of the strength of the spurious currents. To illustrate the performance of the presented MRT-LB model, the MRT-LB models with standard scheme and B-W scheme for both pressure form and potential form of the surface force are implemented to measure the average kinetic energy. From Fig. C.3, we can see that the average kinetic energy with potential form initially decreases at the same rate as that with the pressure form of standard and B-W schemes. Generally, it can be seen that the average kinetic energy of the potential form is smaller than the pressure form. Especially, in the B-W scheme with the potential form, we can get the lowest average kinetic energy among all the noticed schemes. This also means that the spurious currents can be reduced effectively by the B-W scheme with the potential form. Next, to examine the relationship between the value of A and the spurious currents, the average kinetic energy with different values of A is numerically studied by the B-W scheme with potential form. It can be seen from Fig. C.4 that the magnitude of the average kinetic energy is decreased with the decrease of the value of A . However, the computational efficiency is reduced with the decrease of A . To balance the computational efficiency and the accuracy, a moderate value of A should be chose.

In addition, to demonstrate the capability of the proposed LBM, the multiple merging droplets are simulated. Fig. C.5 shows the simulated molar density distribution for the eight droplets case at different

times during the evolution. The eight cubic droplets first evolve into eight separate spheres, then start to merge and finally form one bigger sphere.

4.4. Calculation of surface tension and validation of Young-Laplace law

175 To illustrate that the proposed MRT-LB model can simulate the realistic hydrocarbon species in oil-gas system quantitatively, the surface tensions σ of nC_4 at different temperatures have been computed and compared with previous simulation results and laboratory data. The detailed values of κ , a and the initial values of n_l and n_g for nC_4 at different temperatures are given in Table C.3. While the P-R parameter b is not varied with temperature, its value can be found in Table C.1.

As mentioned in Ref. [31], the surface tension is defined as the net contractive force per unit length of interface, with a unit of N/m . But thermodynamically, it is defined as the work for creating a unit area of interface with a unit of J/m^2 . Using the first law of thermodynamics, the surface tension can be related to the Helmholtz free energy as follows

$$\sigma = \frac{F(n) - F_0(n_{init})}{A} \cong \frac{\int_{\Omega} f_{\text{intfTens}} dx}{A}, \quad (26)$$

with the assumption that σ is spatially constant within the interface for the given system and A is the surface area of the droplet. The surface tension contribution of Helmholtz free energy is defined as

$$f_{\text{intfTens}} = 2f_{\nabla}(n) = \kappa \nabla n \cdot \nabla n.$$

At temperature $T = 333.28K$, $F(n) - F_0(n_{init}) \cong 2.7306 \times 10^{-18}J$. Here, in our numerical experiment, the volume of the drop V is $(0.4 \times L)^3$. After evaluate the radius of the droplet by

$$r = \left(\frac{3}{4\pi}V\right)^{\frac{1}{3}} + L_s, \quad (27)$$

180 where L_s is the width of the two-phase interface. Its definition can be found in Ref. [46]. In our simulations, the surface area of the droplet at $T = 333.28K$ is $A = 4\pi \times (r)^2$. Then, the surface tension can be calculated as $\sigma = 2.7306 \times 10^{-18}/A = 6.543 \times 10^{-3}J/m^2 = 6.543mN/m$. In the same way, the surface tensions at other temperatures can be calculated. The numerical results of σ at different temperatures by the present MRT-LBM are compared with the experimental data and the previous work [31] (see Fig. C.6 (a)). It can
185 be seen that the predicted values agree well with the laboratory data, and it is much more accurate than the results from the two dimensional simulations [31], which do not consider the interfacial thickness.

Next, the well-known Young-Laplace equation is also verified in this work. In the three dimensional simulation, if we assume that the gas bubble has a spherical shape of radius r ,

$$dA = 8\pi r dr, dV = 4\pi r^2 dr.$$

Combining the above equations, the capillary P_c , relates to the surface tension σ , can be written in the following well known Young-Laplace equation ,

$$P_l - P_g = P_c = \sigma dA/dV = 2\sigma/r,$$

where, P_l is the pressure in the center of liquid drop (picked from element (100,100,100)), while P_g is the pressure in the bulk gas region (picked from element (50,50,50)). Here, the thermodynamic pressure of the P-R EOS for the liquid P_l and gas P_g is defined as follows

$$P_{(l \text{ or } g)} = \frac{nRT}{1 - bn} - \frac{n^2 a(T)}{1 + 2bn - b^2 n}, \quad (28)$$

In Fig. C.6 (b), we can clearly see that the capillary pressures of nC_4 predicted by the LBM and those by the Young-Laplace equation are well matched. It is worth mentioning that the results calculated by the Young-Laplace equation in the paper [28] do not match the numerical results because they use the two dimensional
 190 Young-Laplace formula while the numerical experiments are in the three-dimension case. However, in our work, the correct Young-Laplace formula is used, therefore the capillary pressures predicted by the present simulation agree well with those by Young-Laplace equation.

5. Conclusion

Aimed at the realistic two-phase fluid system with P-R EOS, an MRT-LB model with B-W scheme has
 195 been proposed in this paper. In the derivation of the mathematical model for non-ideal fluids with P-R EOS, we first combine the first law of thermodynamics and the related physical relations to derive the entropy balance equation. Then a transport equation of the Helmholtz free energy density is obtained. Furthermore, using the second law of thermodynamics, we derive a more compact formation of hydrodynamic equation (called the potential form), where the nonideal force is directly computed from the Helmholtz free energy
 200 density of P-R fluid.

Furthermore, based on the potential form of the hydrodynamic equation, the proposed MRT-LB model with B-W scheme can eliminate the spurious currents effectively. The multi-scale Chapman-Enskog analysis shows that the second order accuracy can be naturally achieved by this MRT-LB model without any other requirements and numerical boundary conditions. Finally, the three dimensional numerical simulation of
 205 nC_4 shows that the magnitude of spurious currents can be significantly reduced by the the present MRT-LB model when the potential form of surface force is used. Besides, the quantitative numerical results also show that our predictions of surface tension have a better agreement with laboratory data.

Acknowledgments

Z. Qiao's work is partially supported by Hong Kong Research Council GRF grant 15325816. X. Yang's
 210 work is partially supported by the Hong Kong Polytechnic University Postdoctoral Fellowships Scheme 1-YW1D and the Natural Science Foundation of China (Grant No. 11802090).

Appendix A. Parameters of the P-R EOS

The parameters of P-R EOS are defined in a classical way. For pure-component fluid systems, the parameter $a = a(T)$ and b are given by

$$a(T) = 0.45724 \frac{R^2 T_c^2}{P_c} \left(1 + m \left(1 - \sqrt{\frac{T}{T_c}} \right) \right)^2, \quad b = 0.07780 \frac{RT_c}{P_c}.$$

Here, T_c and P_c represent the critical temperature and the critical pressure of a pure substance, respectively. The parameter m is a fitting formula of the acentric factor ω of the substance

$$m = 0.37464 + 1.54226\omega - 0.26992\omega^2, \omega \leq 0.49,$$

$$m = 0.379642 + 1.485030\omega - 0.164423\omega^2 + 0.016666\omega^3, \omega > 0.49.$$

The acentric parameter ω can be computed by using critical temperature T_c , critical pressure P_c and the normal boiling point T_b :

$$\omega = \frac{3}{7} \left(\frac{\log_{10} \left(\frac{P_c}{14.695 \text{ PSI}} \right)}{\frac{T_c}{T_b} - 1} \right) - 1.$$

The definition of parameter κ is related to the P-R parameters a and b by

$$\kappa = ab^{2/3} (m_1^c (1 - \frac{T}{T_c}) + m_2^c),$$

here, m_1^c and m_2^c denote the coefficients which can be related to the acentric factor ω by

$$m_1^c = -\frac{10^{-16}}{1.2326 + 1.3757\omega}, m_2^c = \frac{10^{-16}}{0.9051 + 1.5410\omega}.$$

Appendix B. From MRT-LBE to the Hydrodynamic equations: Multi-scale Chapman-Enskog expansion

Rewritten the evolution equation (20) up to $O(\delta x^3)$, one can obtain the following equation

$$g_i(\mathbf{x}, t + \delta t) = g_i^+(\mathbf{x}, t) - \delta t \mathbf{c} \mathbf{e}_i \cdot \nabla g_i^+(\mathbf{x}, t) + \frac{1}{2} \delta t^2 (\mathbf{c} \mathbf{e}_i \cdot \nabla)^2 g_i^+(\mathbf{x}, t) + O(\delta x^3). \quad (\text{B.1})$$

Multiplying Eq. (17) by inverse of the transformation matrix M , and substituting it into the above equation and expanding the variables around (\mathbf{x}, t) up to $O(\delta x^2)$ and $O(\delta t^2)$, we obtain

$$\partial_t g_i + \mathbf{c} \mathbf{e}_i \cdot \nabla g_i = \Omega_i - \frac{\delta t}{2} [\partial_t^2 g_i - (\mathbf{c} \mathbf{e}_i \cdot \nabla)^2 g_i + 2 \mathbf{c} \mathbf{e}_i \cdot \nabla \Omega_i] + O(\delta x^2 + \delta t^2), \quad (\text{B.2})$$

215 where $\Omega_i = -\Lambda_{ij} (g_j - g_j^{eq}) + G_i$.

$\partial_t^2 g_i$ can be expressed as

$$\partial_t^2 g_i = (\mathbf{c} \mathbf{e}_i \cdot \nabla)^2 g_i + \partial_t \Omega_i - \mathbf{c} \mathbf{e}_i \cdot \nabla \Omega_i + O(\delta t). \quad (\text{B.3})$$

Thus, Eq. (B.2) can be rewritten as

$$D_i g_i = (1 - \frac{\delta t}{2} D_i) \Omega_i + O(\delta x^2 + \delta t^2), \quad (\text{B.4})$$

where $D_i = \partial_t + \mathbf{c}_i \cdot \nabla$.

In addition, from Eq. (B.2), we can see that $\Omega_i = D_i g_i + O(\delta t)$. Thus, Eq. (B.4) is also equivalent to

$$D_i g_i + \frac{\delta t}{2} D_i^2 g_i = -\Lambda_{ij} [g_j - g_j^{eq}] + G_i + O(\delta x^2 + \delta t^2). \quad (\text{B.5})$$

Then we introduce the following expansions:

$$\begin{aligned} g_i &= g_i^{(0)} + \varepsilon g_i^{(1)} + \varepsilon^2 g_i^{(2)} + \dots, \\ \frac{\partial}{\partial t} &= \varepsilon \frac{\partial}{\partial t_1} + \varepsilon^2 \frac{\partial}{\partial t_2}, \quad \nabla = \varepsilon \nabla_1, \quad G_i = \varepsilon G_i^{(1)}, \end{aligned} \quad (\text{B.6})$$

where ε is a small parameter. With the expansions, Eq. (B.5) can be rewritten in consecutive orders of ε as

$$O(\varepsilon^0) : g_i^{(0)} = g_i^{(eq)}, \quad (\text{B.7a})$$

$$O(\varepsilon^1) : D_{1i} g_i^{(eq)} = -\Lambda_{ij} g_j^{(1)} + G_i^{(1)}, \quad (\text{B.7b})$$

$$O(\varepsilon^1) : \partial_{t_2} g_i^{(0)} + D_{1i} [(I_{ij} - \frac{\Lambda_{ij}}{2}) g_j^{(1)}] = -\Lambda_{ij} g_j^{(2)} - \frac{\delta t}{2} D_{1i} G_i^{(1)}, \quad (\text{B.7c})$$

where $D_{1i} = \partial_{t_1} + \mathbf{c}_i \cdot \nabla_1$.

Multiplying the transformation Matrix \mathbf{M} on both side of Eq. (B.7), we can obtain the following moment equations:

$$O(\varepsilon^0) : \mathbf{m}^{(0)} = \mathbf{m}^{(eq)}, \quad (\text{B.8a})$$

$$O(\varepsilon^1) : \mathbf{D}_1 \mathbf{m}^{(0)} = -\tilde{\mathbf{S}} \mathbf{m}^{(1)} + \hat{\mathbf{G}}^{(1)}, \quad (\text{B.8b})$$

$$O(\varepsilon^2) : \partial_{t_2} \mathbf{m}^{(0)} + \mathbf{D}_1 (\mathbf{I} - \frac{\mathbf{S}}{2}) \mathbf{m}^{(1)} + \frac{\delta t}{2} \mathbf{D}_1 \hat{\mathbf{G}}^{(1)} = -\tilde{\mathbf{S}} \mathbf{m}^{(2)}, \quad (\text{B.8c})$$

where $\mathbf{D}_1 = \partial_{t_1} \mathbf{I} + \mathbf{C}_\alpha \partial_{1\alpha}$, \mathbf{C}_α is the discrete velocity matrix.

In addition, from Eqs. (21) and (B.8a), we derive

$$\rho^{(1)} = 0, j_x^{(1)} = -\frac{\delta t}{2} F_{tx}^{(1)}, j_y^{(1)} = -\frac{\delta t}{2} F_{ty}^{(1)}, \rho^{(k)} = j_x^{(k)} = j_y^{(k)} = 0, k > 1. \quad (\text{B.9})$$

On the t_1 time scale, Eq. (B.8b) can be rewritten as follows:

$$\partial_{t_1} \begin{bmatrix} \rho \\ \rho(-2 + 3\mathbf{u}^2) \\ \rho(1 - 3\mathbf{u}^2) \\ \rho u \\ -\rho u \\ \rho v \\ -\rho v \\ \rho(u^2 - v^2) \\ \rho uv \end{bmatrix} + \partial_{1x} \begin{bmatrix} \rho u \\ 0 \\ -\rho u \\ c_s^2 \rho + \rho u^2 \\ \rho B_x/3 \\ \rho uv \\ \rho uv \\ 2\rho u/3 \\ \rho v/3 \end{bmatrix} + \partial_{1y} \begin{bmatrix} \rho v \\ 0 \\ -\rho v \\ \rho uv \\ \rho uv \\ c_s^2 \rho + \rho v^2 \\ \rho B_y/3 \\ -2\rho v/3 \\ \rho u/3 \end{bmatrix} = \begin{bmatrix} 0 \\ -\tilde{s}_1 e^{(1)} \\ -\tilde{s}_2 \varepsilon^{(1)} \\ 0 \\ -\tilde{s}_4 q_x^{(1)} \\ 0 \\ -\tilde{s}_6 q_y^{(1)} \\ -\tilde{s}_7 p_{xx}^{(1)} \\ -\tilde{s}_8 p_{xy}^{(1)} \end{bmatrix} + \begin{bmatrix} 0 \\ 6(1 - s_1/2)\mathbf{u} \cdot \mathbf{F}_t^{(1)} \\ -6(1 - s_2/2)\mathbf{u} \cdot \mathbf{F}_t^{(1)} \\ F_{tx}^{(1)} \\ -(1 - s_4/2)F_{tx}^{(1)} \\ F_{ty}^{(1)} \\ -(1 - s_6/2)F_{ty}^{(1)} \\ 2(1 - s_7/2)(uF_{tx}^{(1)} - vF_{ty}^{(1)}) \\ (1 - s_8/2)(uF_{ty}^{(1)} + vF_{tx}^{(1)}) \end{bmatrix} \quad (\text{B.10})$$

220 where $B_x = -1 + 6v^2 + 3\mathbf{u}^2$, $B_y = -1 + 6u^2 + 3\mathbf{u}^2$.

Similarly, From Eq. (B.8b), the scale equations of conserved quantities ρ , j_x and j_y on the t_2 time scale can be rewritten as

$$\partial_{t_2} \rho = 0. \quad (\text{B.11})$$

$$\begin{aligned} \partial_{t_2}(\rho u) + \frac{1}{6}(1 - \frac{s_1}{2})\partial_{1x}e^{(1)} + (1 - \frac{s_7}{2})(\frac{1}{2}\partial_{1x}p_{xx}^{(1)} + \partial_{1y}p_{xy}^{(1)}) + \frac{\delta t}{2}(1 - \frac{s_1}{2})\partial_{1x}(\mathbf{u} \cdot \mathbf{F}_t^{(1)}) \\ + \frac{\delta t}{2}(1 - \frac{s_7}{2})\partial_{1x}(uF_{tx}^{(1)} - vF_{ty}^{(1)}) + \frac{\delta t}{2}(1 - \frac{s_8}{2})\partial_{1y}(uF_{ty}^{(1)} + vF_{tx}^{(1)}) = 0, \end{aligned} \quad (\text{B.12})$$

$$\begin{aligned} \partial_{t_2}(\rho v) + \frac{1}{6}(1 - \frac{s_1}{2})\partial_{1y}e^{(1)} + (1 - \frac{s_7}{2})(\partial_{1x}p_{xy}^{(1)} - \frac{1}{2}\partial_{1y}p_{xx}^{(1)}) + \frac{\delta t}{2}(1 - \frac{s_7}{2})\partial_{1x}(uF_{ty}^{(1)} + vF_{tx}^{(1)}) \\ + \frac{\delta t}{2}(1 - \frac{s_1}{2})\partial_{1y}(\mathbf{u} \cdot \mathbf{F}_t^{(1)}) - \frac{\delta t}{2}(1 - \frac{s_7}{2})\partial_{1y}(uF_{tx}^{(1)} - vF_{ty}^{(1)}) = 0. \end{aligned} \quad (\text{B.13})$$

To close the hydrodynamic equations at the second order of ε , the terms of $e^{(1)}$, $p_{xx}^{(1)}$ and $p_{xy}^{(1)}$ in Eqs. (B.12) and (B.13) should be estimated. Under the low Mach number assumption, these terms can be evaluated as

$$e^{(1)} = -\frac{1}{\tilde{s}_1}[2\rho(\partial_{1x}u + \partial_{1y}v) + 3s_1\mathbf{u} \cdot \mathbf{F}_t^{(1)}] + O(Ma^3), \quad (\text{B.14})$$

$$p_{xx}^{(1)} = -\frac{1}{\tilde{s}_7}[\frac{2}{3}\rho(\partial_{1x}u - \partial_{1y}v) + s_7(uF_{tx}^{(1)} - vF_{ty}^{(1)})] + O(Ma^3), \quad (\text{B.15})$$

$$p_{xy}^{(1)} = -\frac{1}{\tilde{s}_8}[\frac{1}{3}\rho(\partial_{1x}v + \partial_{1y}u) + \frac{s_8}{2}(uF_{ty}^{(1)} + vF_{tx}^{(1)})] + O(Ma^3). \quad (\text{B.16})$$

With Eqs. (B.14), (B.15) and (B.16), we can obtain the hydrodynamic equations at t_1 and t_2 scales, Continuity equations

$$\partial_{t_1} \rho + \partial_{1x}(\rho u) + \partial_{1y}(\rho v) = 0, \quad (\text{B.17})$$

$$\partial_{t_2} \rho = 0. \quad (\text{B.18})$$

Momentum equations

$$\partial_{t_1}\rho u + \partial_{1x}(c_s^2\rho + \rho u^2) + \partial_{1y}(\rho uv) = F_{tx}^{(1)}, \quad (\text{B.19})$$

$$\partial_{t_1}\rho v + \partial_{1x}(\rho uv) + \partial_{1y}(c_s^2\rho + \rho v^2) = F_{ty}^{(1)}, \quad (\text{B.20})$$

$$\partial_{t_2}(\rho u) = \partial_{1x}(\rho\nu(\partial_{1x}u - \partial_{1y}v) + \rho\zeta(\partial_{1x}u + \partial_{1y}v)) + \partial_{1y}(\rho\nu(\partial_{1x}v + \partial_{1y}u)), \quad (\text{B.21})$$

$$\partial_{t_2}(\rho v) = \partial_{1x}(\rho\nu(\partial_{1x}v + \partial_{1y}u)) + \partial_{1y}(\rho\nu(\partial_{1y}v - \partial_{1x}u) + \rho\zeta(\partial_{1x}u + \partial_{1y}v)), \quad (\text{B.22})$$

where $\nu = \rho\eta$ and $\zeta = \rho\xi$ are the kinematic and bulk viscosities, respectively. In the present MRT-LB model, we enforce $\nu = \frac{1}{3}(\frac{1}{s_7} - \frac{1}{2})\delta t$ and $\zeta = \frac{1}{3}(\frac{1}{s_1} - \frac{1}{2})\delta t$.

Combining the above equations on t_0 and t_1 scale, the following hydrodynamic equations can be obtained.

$$\partial_t\rho + \nabla \cdot (\rho\mathbf{u}) = 0, \quad (\text{B.23})$$

$$\frac{\partial\rho\mathbf{u}}{\partial t} + \nabla \cdot (\rho\mathbf{u} \otimes \mathbf{u}) = -\nabla c_s^2\rho + \nabla \cdot [\rho\nu(\nabla\mathbf{u} + \nabla\mathbf{u}^T) + \rho(\zeta - \nu)(\nabla \cdot \mathbf{u})\mathbf{I}] + \mathbf{F}_t. \quad (\text{B.24})$$

Remark. The above analysis is in the 2D space while we can use the similar technique to analyze the 3D problem through using the D3Q15 model. The transformation matrix of the D3Q15 model and other related parameters are given as follows.

Appendix C. D3Q15 MRT model

The 15 discrete velocities $\{\mathbf{e}_i|i = 0, 1, \dots, 14\}$ of the D3Q15 lattice model are given by

$$\mathbf{e}_i = \begin{bmatrix} 0 & 1 & -1 & 0 & 0 & 0 & 0 & 1 & -1 & 1 & -1 & 1 & -1 & 1 & -1 \\ 0 & 0 & 0 & 1 & -1 & 0 & 0 & 1 & 1 & -1 & -1 & 1 & 1 & -1 & -1 \\ 0 & 0 & 0 & 0 & 0 & 1 & -1 & 1 & 1 & 1 & 1 & -1 & -1 & -1 & -1 \end{bmatrix},$$

and the weight coefficients ω_i are presented as

$$\omega_i = \frac{2}{9}, \omega_{1-6} = \frac{1}{9}, \omega_{7-14} = \frac{1}{72}.$$

The moment vector \mathbf{m} is defined as

$$\mathbf{m} = (\rho, e, \varepsilon, j_x, q_x, j_y, q_y, j_z, q_z, 3p_{xx}, p_{ww}, p_{xy}, p_{zx}, m_{xyz})^T.$$

The non-dimensional relaxation matrix \mathbf{S} is given as

$$\mathbf{S} = \text{diag}(1, s_1, s_2, 1, s_3, 1, s_3, 1, s_3, s_4, s_4, s_4, s_4, s_4, s_5).$$

The transformation matrix \mathbf{M} for the D3Q15-MRT model is a 15×15 matrix, which is given by [47]

$$\mathbf{M} = \begin{bmatrix} 1 & 1 & 1 & 1 & 1 & 1 & 1 & 1 & 1 & 1 & 1 & 1 & 1 & 1 & 1 \\ -2 & -1 & -1 & -1 & -1 & -1 & -1 & 1 & 1 & 1 & 1 & 1 & 1 & 1 & 1 \\ 16 & -4 & -4 & -4 & -4 & -4 & -4 & 1 & 1 & 1 & 1 & 1 & 1 & 1 & 1 \\ 0 & 1 & -1 & 0 & 0 & 0 & 0 & 1 & -1 & 1 & -1 & 1 & -1 & 1 & -1 \\ 0 & -4 & 4 & 0 & 0 & 0 & 0 & 1 & -1 & 1 & -1 & 1 & -1 & 1 & -1 \\ 0 & 0 & 0 & 1 & -1 & 0 & 0 & 1 & 1 & -1 & -1 & 1 & 1 & -1 & -1 \\ 0 & 0 & 0 & -4 & 4 & 0 & 0 & 1 & 1 & -1 & -1 & 1 & 1 & -1 & -1 \\ 0 & 0 & 0 & 0 & 0 & 1 & -1 & 1 & 1 & 1 & 1 & -1 & -1 & -1 & -1 \\ 0 & 0 & 0 & 0 & 0 & -4 & 4 & 1 & 1 & 1 & 1 & -1 & -1 & -1 & -1 \\ 0 & 2 & 2 & -1 & -1 & -1 & -1 & 0 & 0 & 0 & 0 & 0 & 0 & 0 & 0 \\ 0 & 0 & 0 & 1 & 1 & -1 & -1 & 0 & 0 & 0 & 0 & 0 & 0 & 0 & 0 \\ 0 & 0 & 0 & 0 & 0 & 0 & 0 & 1 & -1 & -1 & 1 & 1 & -1 & -1 & 1 \\ 0 & 0 & 0 & 0 & 0 & 0 & 0 & 1 & 1 & -1 & -1 & -1 & -1 & 1 & 1 \\ 0 & 0 & 0 & 0 & 0 & 0 & 0 & 1 & -1 & 1 & -1 & -1 & 1 & -1 & 1 \\ 0 & 0 & 0 & 0 & 0 & 0 & 0 & 1 & -1 & -1 & 1 & -1 & 1 & 1 & -1 \end{bmatrix}.$$

References

- 230 [1] C. Aidun, J. Clausen, Lattice Boltzmann method for complex flows, *Annu. Rev. Fluid Mech.* 42 (2010) 372- 439.
- [2] S. Chen, G. Doolen, Lattice Boltzmann method for fluid flows, *Annu. Rev. Fluid Mech.* 30 (1998) 329-364.
- [3] Z. Guo, C. Shu, Lattice Boltzmann method and its applications in engineering, World Scientific Publishing, Singapore.
- 235 [4] H. Liu, Q. Kang, C. R. Leonardi, S. Schmiechek, Multiphase lattice Boltzmann simulations for porous media applications, *Comput. Geosci* 20 (2016) 777-805.
- [5] P. Randive, A. Dalal, K. C. Sahu, G. Biswas and P. P. Mukherjee, Wettability effects on contact line dynamics of droplet motion in an inclined channel, *Phys. Rev. E*, 91 (2015), 053006.
- [6] P. R. Redapangu, K. C. Sahu, and S. P. Vanda, A study of pressure-driven displacement flow of two
240 immiscible liquids using a multiphase lattice Boltzmann approach, *Phys. Fluids*, 24 (2012) 102110.
- [7] K. C. Sahu, S. P. Vanka, A multiphase lattice Boltzmann simulation of Bouyancy induced mixing in a tilted channel, *Comput. & Fluids*, 50 (2011) 199-215.

- [8] A. Gunstensen, D. Rothman, S. Zaleski, G. Zanetti, Lattice Boltzmann model of immiscible fluids, *Phys. Rev. A* 43 (1991) 4320-4327.
- 245 [9] X. Shan, H. Chen, Lattice boltzmann model for simulating flows with multiple phases and components, *Phys. Rev. E* 47 (1993) 1815-1819.
- [10] X. Shan, H. Chen, Simulation of nonideal gases and liquid gas phase-transition by the lattice Boltzmann equation, *Phys. Rev. E* 49 (1994) 2941-2948.
- [11] M. Swift, E. Orlandini, W. Osborn, J. Yeomans, Lattice Boltzmann simulations of liquid gas and binary
250 fluid systems, *Phys. Rev. E* 54 (1996) 5041-5052.
- [12] M. R. Swift, W. R. Osborn, J. M. Yeomans, Lattice Boltzmann simulation of nonideal fluids, *Phys. Rev. Lett.* 75 (1995) 830-833.
- [13] B. H. Wen, X. Zhou, B. He, C. Y. Zhang and H. P. Fang, Chemical-potential-based lattice Boltzmann method for nonideal fluids, *Phys. Rev. E* 95 (2017) 063305.
- 255 [14] L. Luo, Unified theory of the lattice Boltzmann models for nonideal gases, *Phys. Rev. Lett.* 81 (1998) 1618-1621.
- [15] L. Luo, Theory of the lattice Boltzmann method: Lattice Boltzmann models for nonideal gases, *Phys. Rev. E* (2000) 4982-4996.
- [16] X. He, S. Chen, R. Zhang, A lattice Boltzmann scheme for incompressible multiphase flow and its
260 application in simulations of Rayleigh-Taylor instability, *J. Comput. Phys.* 152 (1999) 652-663.
- [17] T. Lee, C. Lin, A stable discretization of the lattice Boltzmann equation for simulation of incompressible two-phase flows at high density ratio, *J. Comput. Phys.* 206 (2005) 16-47.
- [18] Q. Li, K. H. Luo, Y. J. Gao, Y. L. He, Additional interfacial force in lattice Boltzmann models for incompressible multiphase flows, *Phys. Rev. E* 85 (2012) 026704.
- 265 [19] Y. Wang, C. Shu, H. B. Huang, C. J. Teo, Multiphase lattice Boltzmann flux solver for incompressible multiphase flows with large density ratio, *J. Comput. Phys.* 280 (2015) 404-423.
- [20] H. W. Zheng, C. Shu, Y. T. Chew, A lattice Boltzmann model for multiphase flow with large density ratio, *J. Comput. Phys.* 218 (2006) 353-371.
- [21] D. Anderson, G. McFadden, A. A. Wheeler, Diffuse interface mehtods in fluid mechanics, *Annu. Rev. Fluid Mech.* 30 (1998) 139-165.
270
- [22] D. Jacqmin, Calculation of two-phase Navie-Stokes flows using phase-field modeling, *J. Comput. Phys.* 155 (1999) 96-127.

- [23] Z. H. Chai, D. K. Sun, H. L. Wang, B. C. Shi, A comparative study of local and nonlocal Allen-Cahn equations with mass conservation, *Int. J. Heat Mass Tran.* 22 (2018) 631-642.
- 275 [24] K. Yang, Z. L. Guo, Lattice Boltzmann method for binary fluids based on mass-conserving quasiincompressible phase-field theory, *Phy. Rev. E* 93 (2016) 043303.
- [25] Y. Zu, S. He, Phase-field-based lattice Boltzmann model for incompressible binary fluid systems with density and viscosity contrasts, *Phy. Rev. E* 87 (2013) 043301.
- [26] S. Gong, P. Cheng, Numerical investigation of droplet motion and coalescence by an improved lattice Boltzmann model for phase transitions and multiphase flows, *Comput. & Fluids* 53 (2012) 93-104.
- 280 [27] S. Gong, P. Cheng, A lattice Boltzmann method for simulation of liquid-vapor phase-change heat transfer, *Int. J. Heat Mass Transfer* 55 (2012) 4923-4927.
- [28] H. Li, L. Ju, C. Zhang, Q. Peng, Unconditionally energy stable linear schemes for the diffuse interface model with Peng-Robinson equation of state, *J. Sci. Comput.* 75 (2018) 993-1015.
- 285 [29] Q. Peng, A convex-splitting scheme for a diffuse interface model with Peng-Robinson equation of state, *Adv. Appl. Math. Mech.* 9 (2017) 1162-1188.
- [30] Q. Peng, Z. Qiao, S. Sun, Stability and convergence analysis of second-order schemes for a diffuse interface model with Peng-Robinson equation of state, *J. Comp. Math.* 35 (2017) 737-765.
- [31] Z. Qiao, S. Sun, Two-phase fluid simulation using a diffuse interface model with Peng-Robinson equation of state, *SIAM J. Sci. Comput.* 36 (2014) B708-B728.
- 290 [32] X. Fan, J. Kou, Z. Qiao, S. Sun, A component-wise convex splitting scheme for diffuse interface models with van der Waals and Peng-Robinson equation of state, *SIAM J. Sci. Comput.* 39 (2017) B1-B28.
- [33] J. Kou, S. Sun, Multi-scale diffuse interface modeling of multi-component two-phase flow with partial miscibility, *J. Comput. Phys.* 318 (2016) 349-372.
- 295 [34] J. Kou, S. Sun, and X. Wang, Linearly decoupled energy-stable numerical methods for multicomponent two-phase compressible flow, *SIAM J. Numer. Anal.* 56 (2018) 3219-3248.
- [35] A. Wagner, The origin of spurious velocities in lattice Boltzmann, *Int. J. Mod. Phys. B* 17 (2003) 193-196.
- [36] D. d'Humières, Generalized lattice-Boltzmann equations, in: *Rarefied gas dynamics: Theory and simulations*, Progress in Astronautics and Aeronautics 159 (1992) 450-458.
- 300 [37] P. Lallemand, L. Luo, Theory of the lattice Boltzmann method: Dispersion, dissipation, isotropy, Galilean invariance, and stability, *Phys. Rev. E* 61 (2000) 6546.

- [38] B. Breure, C. J. Peters, Modeling of the surface tension of pure components and mixtures using the density gradient theory combined with a theoretically derived influence parameter correlation, *Fluid Phase Equil.* 334 (2012) 189-196.
- 305 [39] D. Peng, D. Robinson, A new two-constant equation of state, *Ind. Eng. Chem. Fund.* 15 (1976) 59-64.
- [40] T. Lee, P. Fischer, Eliminating parasitic currents in the lattice Boltzmann equation method for nonideal gases, *Phys. Rev. E* 74 (2006) 046709.
- [41] Z. Guo, C. Zheng, T. Zhao, A lattice BGK scheme with general propagation, *J. Sci. Comput.* 16 (2001) 569- 585.
- 310 [42] G. R. McNamara, A. L. Garcia, B. J. Alder, Stabilization of thermal lattice Boltzmann models, *J. Stat. Phys.* 81 (1995) 395-408.
- [43] M. E. McCracken, J. Abraham, Multi-relaxation-time lattice Boltzmann model for multiphase flow, *Phys. Rev. E* 71 (2005) 0367011-9.
- [44] A. Fakhari, T. Lee, Multi-relaxation-time lattice Boltzmann method for immiscible fluids at high
315 Reynolds numbers, *Phys. Rev. E* 87 (2013) 0233041-8.
- [45] A. Firoozabadi, *Thermodynamics of Hydrocarbon Reservoirs*, McGraw-Hill, New York, 1999.
- [46] L. Q. Chen and J. Shen, Applications of semi-implicit Fourier-spectral method to phase field equations, *Comput. Phys. Commun.* 108 (1998) 147-158.
- 320 [47] D. d’Humières, I. Ginzburg, M. Krafczyk, P. Lallemand, L. Luo, Multiple-relaxation-time lattice Boltzmann models in three dimensions, *Phil. Trans. R. Soc. Lond. A* 360 (2002) 437-451.

Table C.1: Relevant data of nC_4 .

T_c , K	P_c , MPa	T_b , K	a	b	κ	n_g	n_l
425.18	3.797	272.64	1.6944	7.2442×10^{-5}	2.0887×10^{-3}	403.17	8878.89

Table C.2: E_ϕ with different lattice spacings and different CFL numbers.

$mesh$	A=1.0		A=0.5		A=0.1		A=0.05	
	E_ϕ	order	E_ϕ	order	E_ϕ	order	E_ϕ	order
128	1.02×10^{-2}	–	9.58×10^{-3}	–	9.14×10^{-3}	–	8.82×10^{-3}	–
256	2.81×10^{-3}	1.8923	2.56×10^{-3}	1.9057	2.43×10^{-3}	1.9112	2.54×10^{-3}	1.9163
512	7.51×10^{-4}	1.9015	6.78×10^{-4}	1.9142	6.48×10^{-4}	1.9069	6.67×10^{-4}	1.9272

Table C.3: Values of κ , a and initial molar densities of nC_4 .

T	a	κ	n_g	n_l
255.02K	2.0020	1.9285×10^{-3}	22.082	1.1274×10^4
270.90K	1.9463	1.9582×10^{-3}	43.757	1.0939×10^4
285.43K	1.8974	1.9834×10^{-3}	71.480	1.0639×10^4
299.48K	1.8519	2.0060×10^{-3}	109.81	1.0321×10^4
315.82K	1.8010	2.0302×10^{-3}	173.08	0.9912×10^4
333.28K	1.7487	2.0536×10^{-3}	270.37	0.9419×10^4

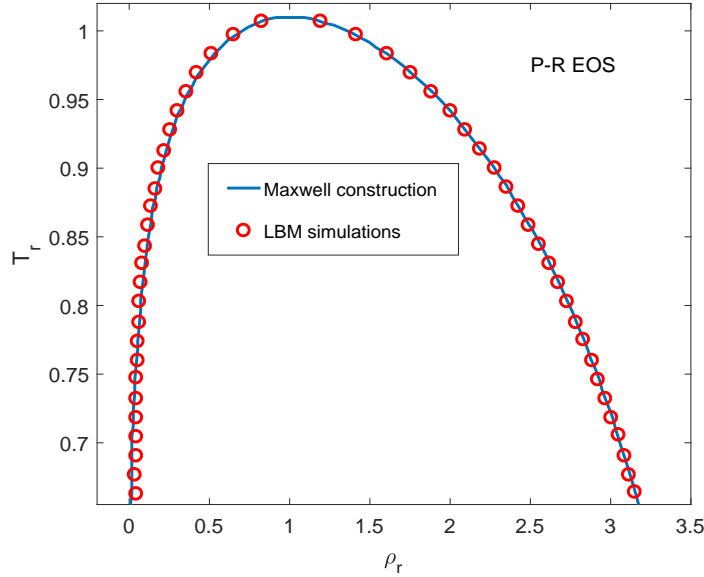


Figure C.1: Two phase coexistence curve.

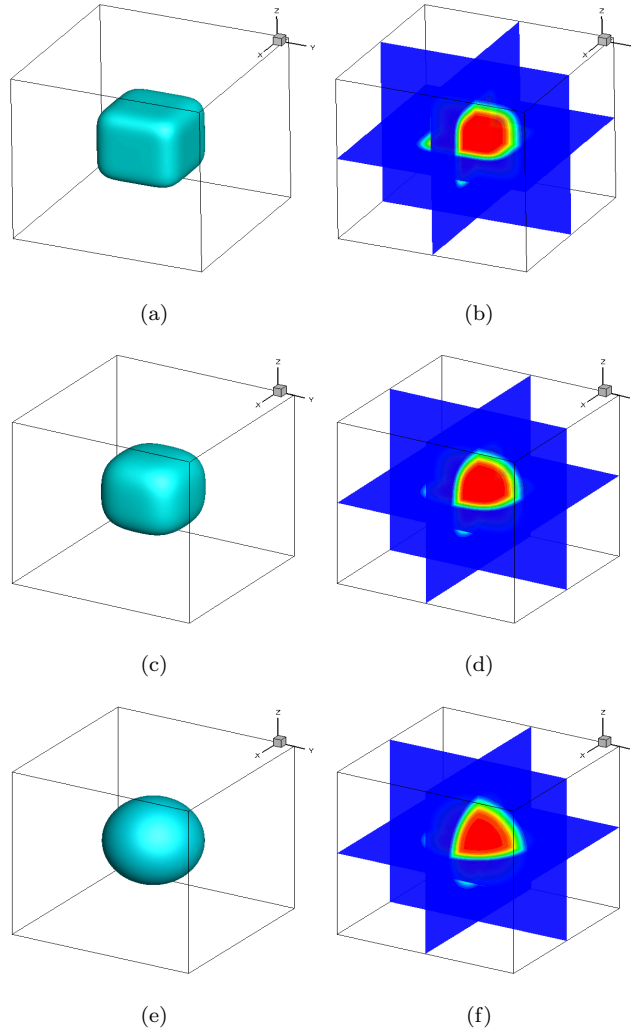


Figure C.2: Time evolution of the molar density distribution; (a) $t = 200$, (b) $t = 500$, (c) $t = 1000$.

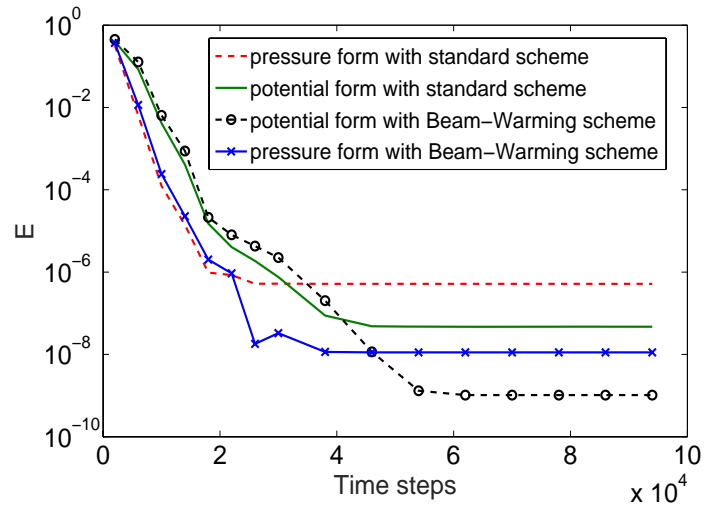


Figure C.3: Time history of the average kinetic energy.

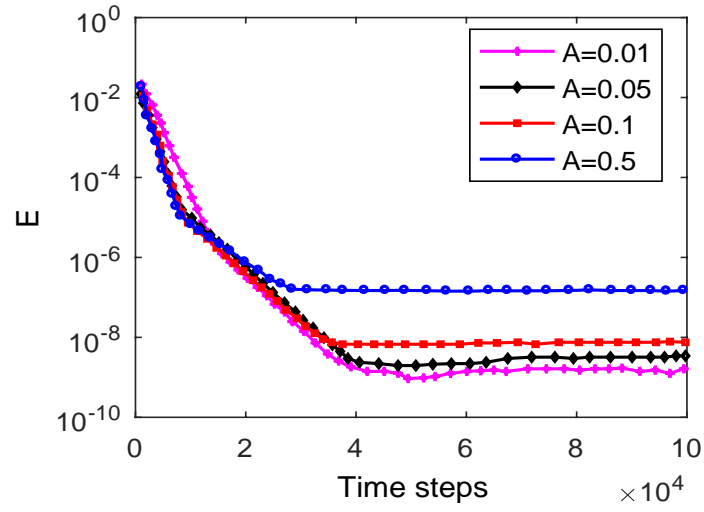


Figure C.4: Time history of the average kinetic energy with different CFL numbers.

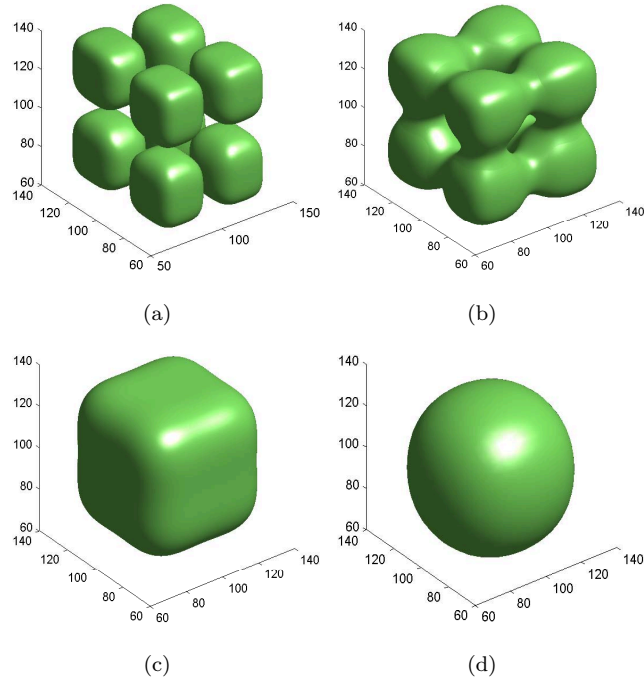


Figure C.5: Time evolution of the multiple merging droplets; (a) $t = 100$, (b) $t = 400$, (c) $t = 1000$, (d) $t = 2000$.

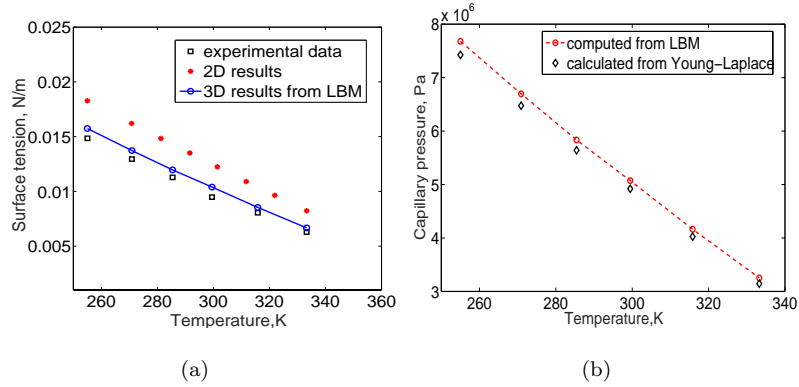


Figure C.6: Numerical validation: (a) Comparison of surface tension, (b) validation of Laplace law.